

# GPS slant total electron content accuracy using the single layer model under different geomagnetic regions and ionospheric conditions

C. Brunini · F. Azpilicueta

Received: 17 April 2009 / Accepted: 14 January 2010 / Published online: 29 January 2010  
© Springer-Verlag 2010

**Abstract** The use of observations from the Global Positioning System (GPS) has significantly impacted the study of the ionosphere. As it is widely known, dual-frequency GPS observations can provide very precise estimation of the slant Total Electron Content (sTEC—the linear integral of the electron density along a ray-path) and that the precision level is bounded by the carrier-phase noise and multi-path effects on both frequencies. Despite its precision, GPS sTEC estimations can be systematically affected by errors in the estimation of the satellites and receivers by Inter-Frequency Biases (IFB) that are simultaneously determined with the sTEC. Thus, the ultimate accuracy of the GPS sTEC estimation is determined by the errors with which the IFBs are estimated. This contribution attempts to assess the accuracy of IFBs estimation techniques based on the single layer model for different ionospheric regions (low, mid and high magnetic latitude); different seasons (summer and winter solstices and spring and autumn equinoxes); different solar activity levels (high and low); and different geomagnetic conditions (quiet and very disturbed). The followed strategy relies upon the generation of a synthetic data set free of IFB, multi-path, measurement noise and of any other error source. Therefore, when a data set with such properties is used as the input of the IFB estimation algorithms, any deviation from zero on the estimated IFBs should be taken as indications of the errors introduced by the estimation technique. The truthfulness of

this assessment work is warranted by the fact that the synthetic data sets resemble, as realistically as possible, the different conditions that may happen in the real ionosphere. The results of this work show that during the high solar activity period the accuracy for the estimated sTEC is approximately of  $\pm 10$  TECu for the low geomagnetic region and of  $\pm 2.2$  TECu for the mid-latitude. During low solar activity the accuracy can be assumed to be in the order of  $\pm 2$  TECu. For the geomagnetic high-disturbed period, the results show that the accuracy is degraded for those stations located over the region where the storm has the strongest impact, but for those stations over regions where the storm has a moderate effect, the accuracy is comparable to that obtained in the quiet period.

**Keywords** GPS · Slant total electron content (sTEC) · Inter-frequency biases (IFB) · sTEC calibration

## 1 Introduction

It is widely known that dual-frequency GPS observations can provide very precise estimation of the slant Total Electron Content (sTEC), i.e. the linear integral of the electron density along any satellite-receiver ray path (e.g. [Davies and Hartmann 1997](#); [Manucci et al. 1999](#)) and that the precision level is bounded by the carrier-phase noise and multi-path effects on both frequencies, whose combined effect on the sTEC may reach a few tenths of Total Electron Content units (TECu,  $1 \text{ TECu} = 10^{16}$  electrons per square meter). Despite its precision, GPS sTEC estimations can be systematically affected by errors in the estimation of the inter-frequency biases (IFB) that are simultaneously determined with the sTEC ([Goposchkin and Coster 1992](#)). These biases arise from frequency-dependent delays produced by the hardware and the firmware of

C. Brunini · F. Azpilicueta (✉)  
Facultad de Ciencias Astronómicas y Geofísicas,  
Universidad Nacional de La Plata, Paseo del Bosque,  
1900 La Plata, Argentina  
e-mail: azpi@fcaglp.unlp.edu.ar

C. Brunini · F. Azpilicueta  
Consejo Nacional de Investigaciones Científicas y Tecnológicas  
(CONICET), La Plata, Argentina

the satellites and the receivers (Gao 2008; Schaer 2008). Both together, satellite and receiver IFBs may reach values of several tens of nanoseconds, which would represent a sTEC error of 100 TECu (Sardon et al. 1994). Therefore, in order to get accurate sTEC estimations it is needed to carefully estimate the IFB.

The accuracy of the GPS TEC estimations (either the slant TEC or its derived product, the vertical TEC) has been assessed by means of intra- and inter-technique comparisons. In the first case, the GPS TEC estimations obtained by different groups are compared among themselves (Hernández-Pajares et al. 2008); in the second one, the GPS TEC estimation is compared to values estimated by other instruments, e.g. the Navy Navigation Satellite System (Ciraolo and Spalla 1997), the TOPEX or Jason1 dual-frequency space-born radars (Ho et al. 1997; Azpilicueta and Bruini 2008), ionosondes (Belehaki et al. 2003; Mosert et al. 2007), etc. Nevertheless, both comparison approaches have drawbacks: intra-technique comparisons could be misleading because the different sTEC estimations are highly correlated due to the use of the same data source and/or similar modeling approaches; while inter-technique comparisons are biased by the systematic errors that affect the different instruments. Besides, the GPS TEC estimations have also been compared to predictions from ionospheric models such as the International Reference Ionosphere (Bilitza et al. 1998; Jakowski et al. 1998) or NeQuick (Jodogne et al. 2004; Nava et al. 2005). However, these models are not designed to predict the day-to-day variability of the ionosphere and hence cannot be taken as ground truth for assessing the accuracy of GPS TEC estimates.

The ultimate accuracy of the GPS sTEC estimation is determined by the errors with which the IFBs are estimated. Brunini and Azpilicueta (2009) presented a method for assessing the accuracy of the IFB obtained with a given estimation technique. That method relies upon the generation of a synthetic data set free of IFB, multi-path, measurement noise and of any other error source. When a data set with such properties is used as the input of the IFB estimation technique, the estimated IFB should equal zero. Any deviation from zero should be taken as indications of the errors caused by the estimation technique. The truthfulness of this assessment technique depends on the ability to create synthetic data sets that can resemble, as realistically as possible, the different conditions that may happen in the real ionosphere. Brunini & Azpilicueta's method is based on the use of the NeQuick ionospheric model (Radicella and Leitinger 2001), modified so to use an effective ionization index updated with actual GPS observations. For more details concerning this method and its capability to create realistic ionospheric scenarios, the reader is referred to the paper mentioned above.

Based on the use of Brunini & Azpilicueta's method, this contribution assesses the errors that occur on the estimated

IFBs when the widely applied ionospheric single layer model is used for different ionospheric regions (low, mid and high magnetic latitude); different seasons (summer and winter solstices and spring and autumn equinoxes); different solar activity levels (high and low); and different geomagnetic conditions (quiet and very disturbed). Besides, attention is given to the influence of a critical parameter of the model which is the height of the layer (see Sect. 2.2).

## 2 Analysis method

### 2.1 Error assessment technique by using synthetic data sets

The observation equation that links the sTEC to the GPS observations reads (Ciraolo et al. 2007)

$$L_{R,S} = \text{sTEC} + b_R + b_S + \varepsilon_{R,S}, \quad (1)$$

where  $L_{R,S}$  is the geometry free combination of the carrier phase observations on both GPS frequencies from the receiver  $R$  to the satellite  $S$ ;  $b_R$  and  $b_S$  are the receiver and the satellite IFB assumed as constant for a given period (Bishop et al. 1994); and  $\varepsilon_{R,S}$  encompasses all the un-modeled errors such as carrier-phase measurement noise and multi-path. In Eq. (1) it's assumed that the carrier phase ambiguity effects on the geometry free combination have been removed from the left-hand side term, for example by applying the so-called carrier-to-code leveling process (Manucci et al. 1999). Therefore, the error term  $\varepsilon$  could also contain a contribution due to the errors in the carrier phase ambiguities estimation process. All the terms in Eq. (1) are expressed in TECu.

A data set of synthetic (simulated) observations free of errors and biases was created by using the NeQuick ionospheric model following Brunini and Azpilicueta (2009). In this work, the synthetic observation is computed with the following expression:

$$\tilde{L}_{R,S} = \int_{\Gamma} N_e(\varphi, \lambda, h, t, A_Z) d\gamma, \quad (2)$$

where  $N_e(\varphi, \lambda, h, t, A_Z)$  is the NeQuick electron concentration distribution as a function of the geographic latitude  $\varphi$ , geographic longitude  $\lambda$ , height  $h$  above the Earth's surface, Universal Time  $t$ , and effective ionization index  $A_Z$ . The integral extends along the satellite-receiver ray-path  $\Gamma$  and  $d\gamma$  is a differential of it.

As explained by Nava et al. (2005), the effective ionization index is the main NeQuick driver. Brunini and Azpilicueta (2009) modified the NeQuick model in such a way that the effective ionization index is updated by means of a Kalman filter that ingests actual GPS observations into the model; thus reproducing in a more realistic way the actual electron density behavior.

If the term for the actual observation in Eq. (1) (the left-hand term) is replaced by the synthetic one given by Eq. (2), the result is:

$$\tilde{L}_{R,S} = s\tilde{\text{TEC}} + \tilde{b}_R + \tilde{b}_S + \tilde{\varepsilon}_{R,S}. \tag{3}$$

Since the left-hand side term of Eq. (3) is free of errors and biases, any bias estimation technique applied to these data should give:  $\tilde{b}_R = 0, \tilde{b}_S = 0, \tilde{\varepsilon}_{R,S} = 0$  and  $s\tilde{\text{TEC}} = \tilde{L}_{R,S}$ . Therefore, any deviation from these expected results can be taken as indicators of errors in the estimation technique. According to Eq. (3), positive values of  $\tilde{b}_R + \tilde{b}_S$  indicate that the sTEC are underestimated and vice versa.

### 2.2 IFB estimation technique

In the process of determining the values of the IFB of Eq. (1), most of the widely known estimation techniques made use of the so-called ionospheric single layer model (SLM) and its associated mapping function (Manucci et al. 1999; Hernández-Pajares et al. 2008; Gao 2008; Schaer 2008; Brunini and Azpilicueta 2009). This model represents the ionosphere as a shell of infinitesimal thickness at a certain height above the Earth’s surface and relates the sTEC with the vertical TEC (vTEC, the linear integral of the electron density in the radial direction) at the point in which the ray-path intersects the layer (also named as the ionospheric piercing point, IPP), by a so-called mapping function given by the expression

$$\frac{v\tilde{\text{TEC}}}{s\tilde{\text{TEC}}} \cong \cos z' = \sqrt{1 - \left(\frac{R}{R+H}\right)^2 \cdot \cos^2(z)}, \tag{4}$$

where  $R$  is the mean Earth’s radius,  $H$  is the height of the thin layer, and  $z$  and  $z'$  are the satellite zenith distance at the observation point and at the IPP respectively (see Fig. 1).

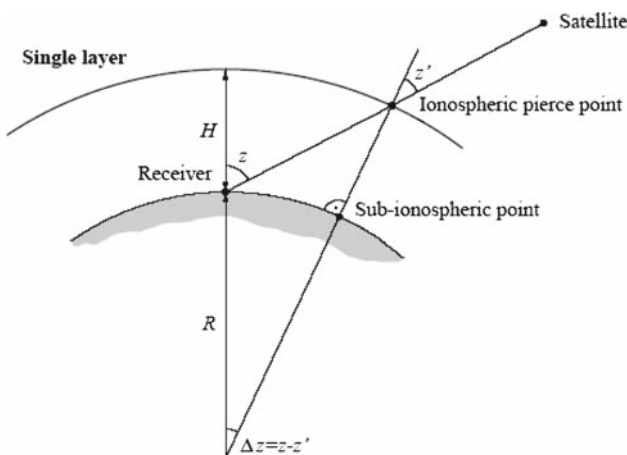


**Fig. 1** schematic representation of the single layer model and the geometric principle of the mapping function extracted from Schaer (1999)

The following step in this type of calibration techniques consists of assuming a mathematical function to represent the spatial and temporal variability of the vTEC. This function depends on whether the calibration is applied to a single station or simultaneously to a set of several stations distributed over a certain region; for example the usual approach for a world-wide adjustment is a set of spherical harmonics functions (Schaer 2008). In this work, we follow Brunini and Azpilicueta (2009), in which the calibration is done on a station-by-station basis and for this the spatial and temporal variability of the vTEC is represented by a bi-linear expansion on the IPP coordinates with time dependent coefficients

$$v\tilde{\text{TEC}} = a_{0,0}(t) + a_{1,0}(t) \cdot x + a_{0,1}(t) \cdot y, \tag{5}$$

where  $t$  is the Universal Time and  $x$  and  $y$  are defined by the relations  $x = (\lambda_{IPP} - \lambda_R) \cdot \cos(\varphi)$  and  $y = \mu_{IPP} - \mu_R$ ,  $\lambda$  being the geographic longitude,  $\varphi$  the geographic latitude, and  $\mu$  the modified dipolar (modip) latitude. The sub-index IPP refers to the IPP location and  $R$  refers to the receiver location. The time-dependent coefficients are mathematically represented by stepwise functions of the form  $a_{i,j}(t) = \alpha_{i,j,k}$ , where  $\alpha_{i,j,k}$  is constant in the interval  $[t_k, t_k + \Delta t)$  and  $\Delta t$  is the refreshing interval.

The modip latitude was firstly proposed by Rawer (1984) for modeling the F2-layer and the top-side ionosphere and it is defined by the relation  $\tan(\mu) = I/\sqrt{\cos(\varphi)}$ , where  $I$  is the magnetic dip at the IPP. For details concerning the benefits of using modip in the representation of the vTEC, the interested reader is referred to Azpilicueta et al. (2005).

Combining Eqs. (3)–(5), the observation equation of the problem results in:

$$\tilde{L}_{R,S} = \sec(z') \cdot [\alpha_{0,0,k} + \alpha_{1,0,k} \cdot x + \alpha_{0,1,k} \cdot y] + \tilde{\beta}_{R,S} + \tilde{\varepsilon}_{R,S}, \tag{6}$$

for  $t_k \leq t < t_k + \Delta t$ , where  $\tilde{\beta}_{R,S} = \tilde{b}_R + \tilde{b}_S$ .

All the observation equations for a pre-defined time interval  $\Delta T$  are arranged in a linear system that contains  $m_C = 3 \cdot \frac{\Delta T}{\Delta t}$  unknowns of the type  $\alpha_{i,j,k}$ , plus  $m_S$  (the number of observed satellites) unknowns of the type  $\tilde{\beta}_{R,S}$ . Provided that the number of observations,  $m_O$ , is greater than the number of unknowns,  $m_U = m_C + m_S$ , the resulting linear system can be solved by the Least Squares method.

According to Sect. 2.1, the  $\tilde{\beta}_{R,S}$  Least Squares estimates should be taken as the errors on the IFB estimations attributed to the calibration technique. Those errors are caused, basically, by two different sources: the mapping function expressed by Eq. (4) and the mathematical expansion of Eq. (5) used to represent the spatial and the temporal variations of the vTEC. The effect of both error sources is relatively low at mid geomagnetic latitudes, but in the low and high geomagnetic regions, the effect becomes significant.

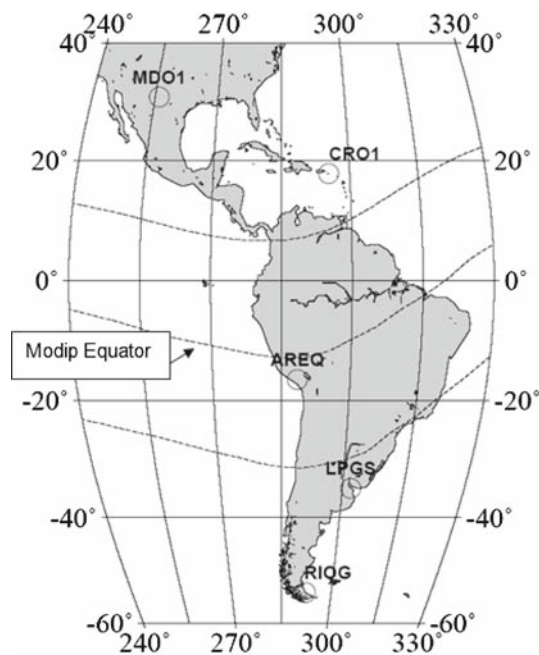


**Fig. 2** Location of the sites analyzed in this work and traces of modip equator and  $\pm 30^\circ$  parallels (the free availability of the GMT software used to draw this figure is acknowledged)

### 3 Results and discussions

#### 3.1 Studied cases

This study analyzed the behavior of the IFB calibration technique at five sites over the American continent, located under different geomagnetic conditions: Arequipa (AREQ;  $\lambda = -71.5^\circ$ ,  $\varphi = -16.5^\circ$ ,  $\mu = -8.2^\circ$ ) in the low latitude region La Plata (LPGS; ( $\lambda = -57.9^\circ$ ,  $\varphi = -34.9^\circ$ ,  $\mu = -36^\circ.7$ ) and Christiansted, Virgin Islands, (CRO1,  $\lambda = -64.5^\circ$ ,  $\varphi = 17.8^\circ$ ,  $\mu = 38.3^\circ$ ) in the mid latitude regions; Río Grande (RIOG;  $\lambda = -67.8^\circ$ ,  $\varphi = -53.8^\circ$ ,  $\mu = -49.7^\circ$ ) and Fort Davis (MDO1,  $\lambda = -104.0^\circ$ ,  $\varphi = 30.7^\circ$ ,  $\mu = 47.9^\circ$ ) in the high latitude regions. Figure 2 shows the location of the sites as well as the traces of the modip equator with the  $\pm 30^\circ$  modip parallels that roughly delimit the low geomagnetic latitude region.

The study comprised the year 2001, which approximately coincides with the maximum of the last solar cycle, with F10.7 index varying between 114 and 284 Solar Flux units (SFu) (see [http://www.drao-ofr.hia-ihh.nrc-cnrc.gc.ca/icarus/www/sol\\_home.shtml](http://www.drao-ofr.hia-ihh.nrc-cnrc.gc.ca/icarus/www/sol_home.shtml)); and the year 2007 close to the minimum of the same solar cycle with F10.7 index varying between 67 and 91 SFu. In both cases, the four seasons of the year were considered: Autumn Equinox (March); Winter Solstice (June); Spring Equinox (September); and Summer Solstice (December). In all the cases above mentioned the geomagnetic activity was quiet with the Dst

geomagnetic index greater than  $\sim 50$  nano-Tesla (nT) (see <http://swdcwww.kugi.kyoto-u.ac.jp/dstdir/finalprov.html>).

In order to assess the effects of a geomagnetic storm on the IFB estimation, the October 2003 super storm (the so-called Halloween storm) was analyzed. During this storm the Dst values dropped to approximately  $-400$  nT and the F10.7 index increased from 243 to 314 SFu (Sahai et al. 2005). For this analysis, the results of the IFB estimation technique for a quiet period (with  $Dst \gg -50$  nT and  $F10.7 = 112$  SFu) close to the storm, were taken as a reference for comparison.

According to Sect. 2.2, a critical error affecting the thin layer ionospheric model is the mapping function used to convert slant to vertical TEC values at the IPP given by Eq. (4). This approximation assumes a spherically stratified ionosphere, which could be a plausible approximation at mid latitude but it is certainly unreliable at low latitude. The errors caused by the presence of horizontal gradients in the electron density distribution can be smaller or larger depending on the adopted thin layer height (Conker and El-Arini 1998). In order to investigate the influence of this parameter on the IFB estimation, two typically used heights were tested:  $H = 450$  and  $H = 350$  km.

All the studied cases comprised the analysis of three consecutive days of synthetic sTEC data that resembled the actual ionospheric conditions present at the given locations and times. Every observation recorded by the GPS receivers has a corresponding observation in the synthetic data set. The objective of this procedure was to reproduce as much as possible a real situation. This means that the data gaps present in the real data files were also included in the synthetic data files with the objective of reproducing the real data file structure. The sampling rate for the synthetic observations is 30 sec and the elevation cutoff mask is  $10^\circ$ . The refreshing interval for the IFB estimation technique is  $\Delta t = 300$  s, which leads to  $m_C = 2,592$  unknowns of the type  $\alpha_{i,j,k}$  for an observation interval  $\Delta T = 259,200$  sec (see Sect. 2.2). Table 1 presents the main characteristics of the samples analyzed in this work. As an order of magnitude, the 3-day data package for every station contains an average of 60,000 measurements.

#### 3.2 Results

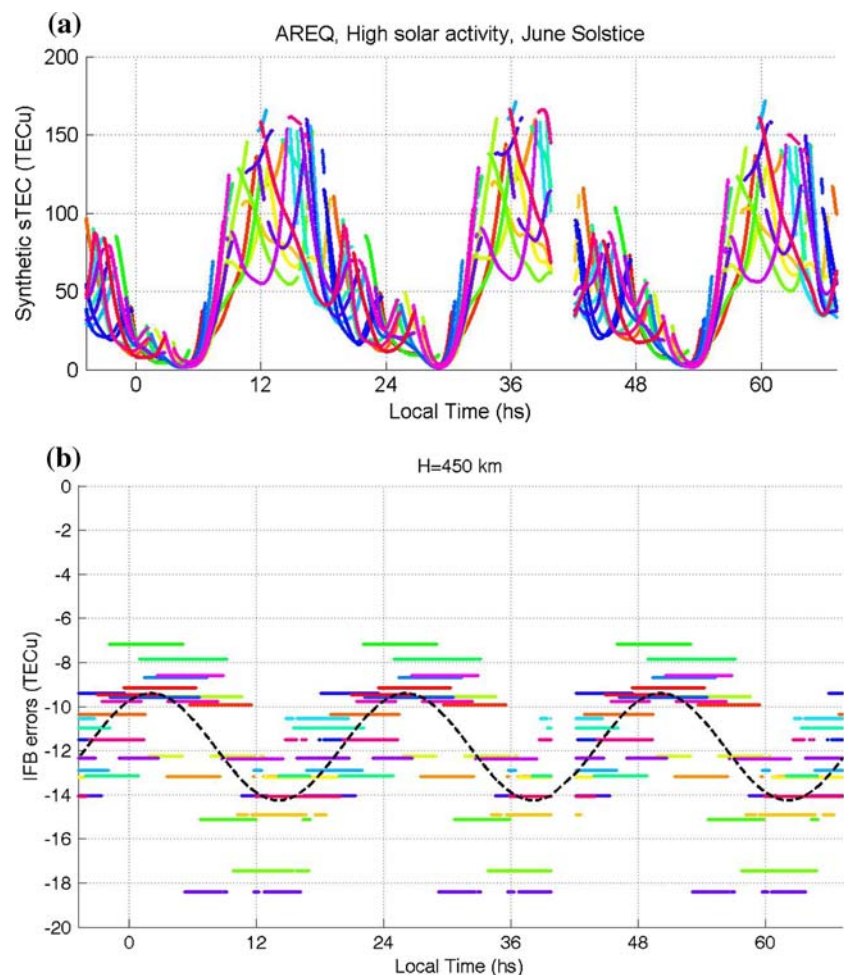
##### 3.2.1 Quiet geomagnetic activity period

According to Sect. 2.1, the Least Squares estimates of the  $\beta_{R,S}$  unknowns should be taken as the IFB errors attributed to the calibration technique described in Sect. 2.2, since by construction the synthetic data have IFBs equal to zero. After Eq. (6), a positive value of  $\tilde{\beta}_{R,S}$  indicates an underestimation on the sTEC, while a negative value indicates an overestimation on them. Figures 3, 4 and 5 show some illustrative cases selected from the samples analyzed in this work: panel

**Table 1** Main characteristic of the samples used in this work (F10.7 is the solar activity characterized by the F10.7 solar index in SFu)

Period	Season	Date	GPS Day	F10.7
High solar activity 2001	Autumn Equinox	March 15–17	074–076	137
	Winter Solstice	June 22–24	173–175	203
	Spring Equinox	September 19–21	262–264	222
	Summer Solstice	December 06–08	340–342	231
Low solar activity 2007	Autumn Equinox	March 15–17	074–076	69
	Winter Solstice	June 16–18	167–169	68
	Spring Equinox	September 16–18	259–261	67
	Summer Solstice	December 21–23	355–357	71
Storm 2003	–	October 29–31	302–304	243–314
Quiet 2003	–	October 08–10	281–283	112

**Fig. 3** Synthetic dataset for AREQ, during the high solar activity year and the winter Solstice (*panel a*) and IFB errors estimated using a thin layer height of 450 km (*panel b*); different colors correspond to different satellites

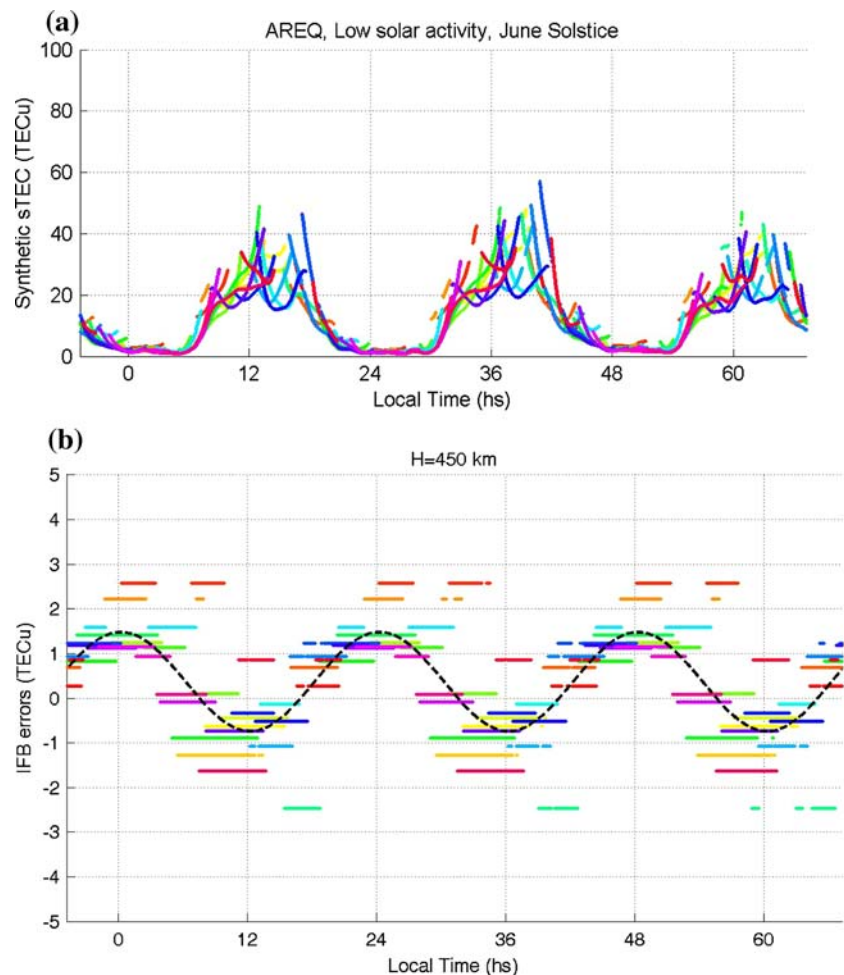


(a) of every figure shows the synthetic data set, i.e.  $\tilde{L}_{R,S}$  in Eqs. (3) and (6); and panel (b) shows the estimated IFB,  $\tilde{\beta}_{R,S}$  in Eq. (6), determined for the different satellites (each color corresponds to a different satellite).

Figure 3 represents what could be considered the worst case found in the sample analyzed in the present work. It corresponds to the low latitude site, for the winter solstice

(seasons correspond to the Southern Hemisphere) of the high solar activity year, using a thin layer height— $H$  in Eq. (4)—of 450 km. The remarkable feature in panel (b) is a large over-estimation of the sTEC for all the observed satellites, which is evidenced by negative IFB errors ranging from  $-18.4$  to  $-7.2$  TECu. Another interesting feature in panel (b) of the figure is a daily signal almost in phase opposition with the

**Fig. 4** Synthetic dataset for AREQ, during the low solar activity year and the winter Solstice (*panel a*) and IFB errors estimated using a thin layer height of 450 km (*panel b*); different colours correspond to different satellites



sTEC variability depicted in panel (a). The Least Squares adjustment of a mean value plus a 24-h periodic signal (represented with the dashed line) provided a mean value of  $-11.8$  TECu and amplitude of  $2.4$  TECu. This daily signal is present in most samples analyzed in this work. Its amplitude varies from  $0.3$  to  $2.7$  TECu, representing a rather small contribution to the IFB error budget, and it is approximately in phase opposition with the sTEC daily variation.

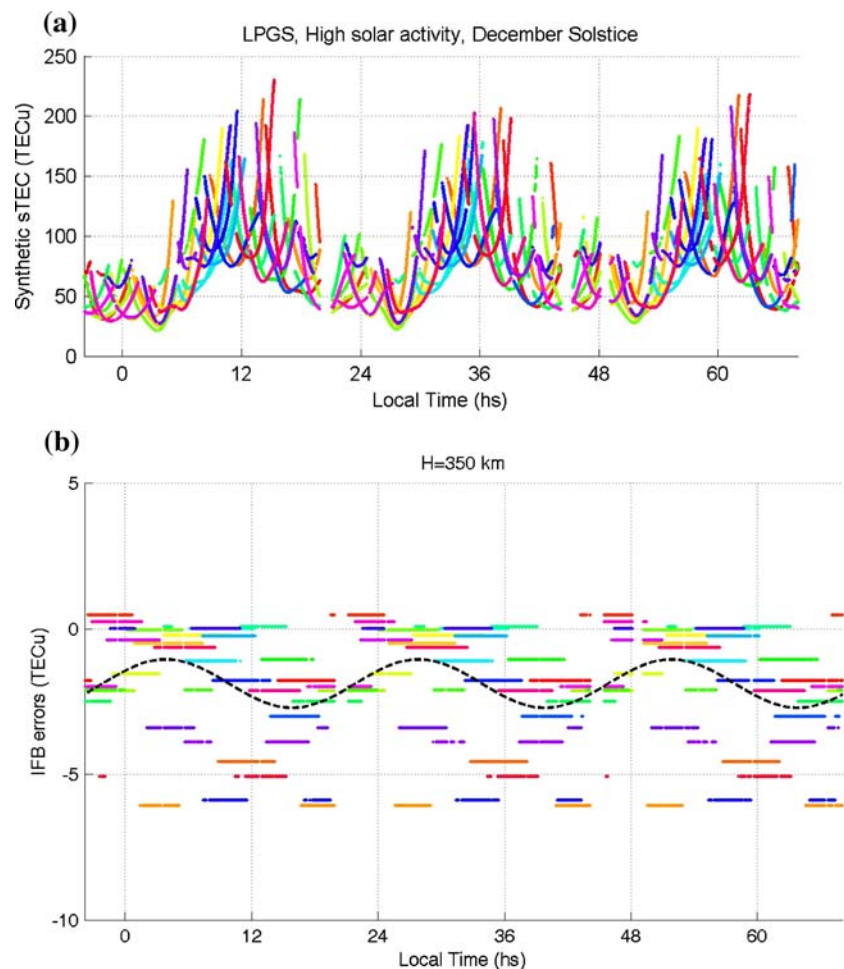
Just for comparison purpose, Fig. 4 shows the equivalent plots for the low solar activity year (please, note the change in the scale of the y-axis of this figure w.r.t. Fig. 3). It can be appreciated that the IFB estimation performs much better for low than for high solar activity. The panel (a) shows a significant decrease on the sTEC values in response to the decline of the F10.7 solar index. The panel (b) shows IFB errors approximately distributed around 0 and ranging from  $-2.5$  to  $2.6$  TECu. The daily signal correlated with the sTEC is still present but its mean value of  $0.4$  TECu and its amplitude of  $1.1$  TECu are much lower than the corresponding values for the high solar activity period.

Figure 5 represents what could be considered the intermediate case found in the sample analyzed in the present work.

It corresponds to the mid latitude site, for the summer solstice of the high solar activity year, using a thin layer height of  $350$  km. In this case, there is also a general overestimation of the sTEC values evidenced by the negative IFB errors ranging from  $-6.1$  to  $+0.5$  TECu as well as a daily signal in phase opposition with the sTEC with a mean value of  $-1.9$  TECu and amplitude of  $0.5$  TECu.

The main results obtained for a quiet geomagnetic period are summarized in Fig. 6. It was constructed based on the percentage of observations affected by a given IFB error in respect of the total number of observations. Since every satellite is affected for the same IFB error, that percentage is identical to the percentage of observations belonging to each satellite. The circles represent the average IFB error and the bars represent the IFB error interval that contains 95% of the observations. While the average IFB error provides an overview of the general over- or underestimation that can be expected in the different cases analyzed in this work, the larger (in absolute value) limit of the IFB error interval gives an estimate of the larger over- or underestimation that can be expected for a given satellite present in the sample.

**Fig. 5** Synthetic dataset for LPGS, during the high solar activity year and the summer Solstice (*panel a*) and IFB errors estimated using a thin layer height of 350 km (*panel b*); different colors correspond to different satellites



The relevant features that can be extracted from Fig. 6 after the analysis of the parameters mentioned above indicate that:

- IFB errors are, in general, negative, which corresponds to overestimated sTEC; the worst values for the lower limit of the IFB error interval found in this work are  $-7.9$  TECu for MDO1,  $-15.4$  TECu for CRO1,  $-18.5$  TECu for AREQ,  $-11.6$  TECu for LPGS and  $-8.2$  TECu for RIOG;
- IFB errors are roughly between 1.5 and 2 times greater for AREQ than for the other analyzed sites;
- In general, there are not significant differences between IFB errors for equinoxes and solstices; except for the case of CRO1 that shows comparatively larger errors during the December than during the other periods.
- There are not any significant differences when comparing the results from the conjugate sites: MDO1—RIOG; CRO1—LPGS.
- The thin layer height parameter has a significant effect on the IFB errors for AREQ during the high solar activity period;  $H = 350$  km performs better than  $H = 450$  km. This behavior is also found in the other sites but the effect

is not as significant as in the first site. During the low solar activity period the results appear similar for both values of the height, independently from the analyzed region.

### 3.2.2 Storm period

The analysis described in the previous section was repeated for the storm period. Figures 7 and 8 show the results obtained for LPGS and MDO1 respectively for the storm period. Panels a) show the synthetic data set and panels b) the IFB errors estimated using a thin layer height of 350 km. For comparison purposes, panels c) and d) of the each figure show the results obtained when the same procedure was applied to a data set, corresponding to a quiet geomagnetic period, few days before the storm. The effects of the super storm on the synthetic sTEC are quite evident if the data set for the storm period is compared to the corresponding quiet one. For example, for the quiet period few days before the storm, typical values for the sTEC over MDO1 for noon time were around 110 TECu (Fig. 8, panel c), and during the storm, the sTEC reached values of more than 300 TECu (Fig. 8, panel d).

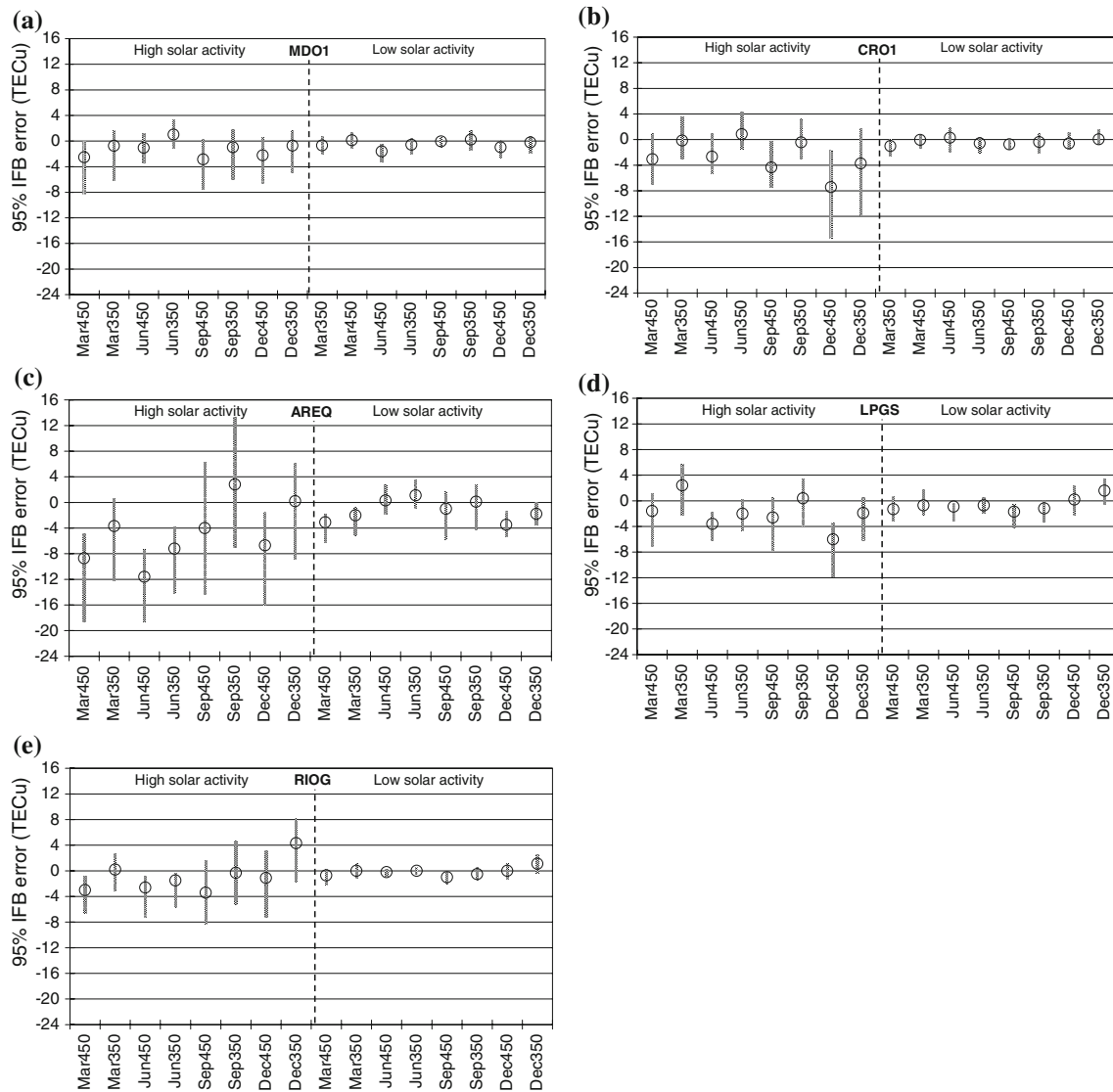


**Fig. 6** Average IFB error (*circles*) and IFB error interval that contains 95% of the observations (*bars*) for the quiet period for: **a** MDO1, **b** CRO1, **c** AREQ, **d** LPGS and **e** RIOG. The *x*-axis shows the month and the layer height

The analysis of the effect of the storm on the IFB determination shows a clear distinction between what is seen over MDO1 (North America) and over LPGS (South America). For MDO1 the errors on the IFB during the storm are significantly larger (between  $-13$  and  $5$  TECu) than those during the quiet period (between  $-2$  and  $1$  TECu). In contrast to this, the results for LPGS show that the IFB errors are slightly larger for the storm (between  $-2.1$  to  $5.2$  TECu) than for the quiet period ( $-3.8$  to  $+2.2$  TECu).

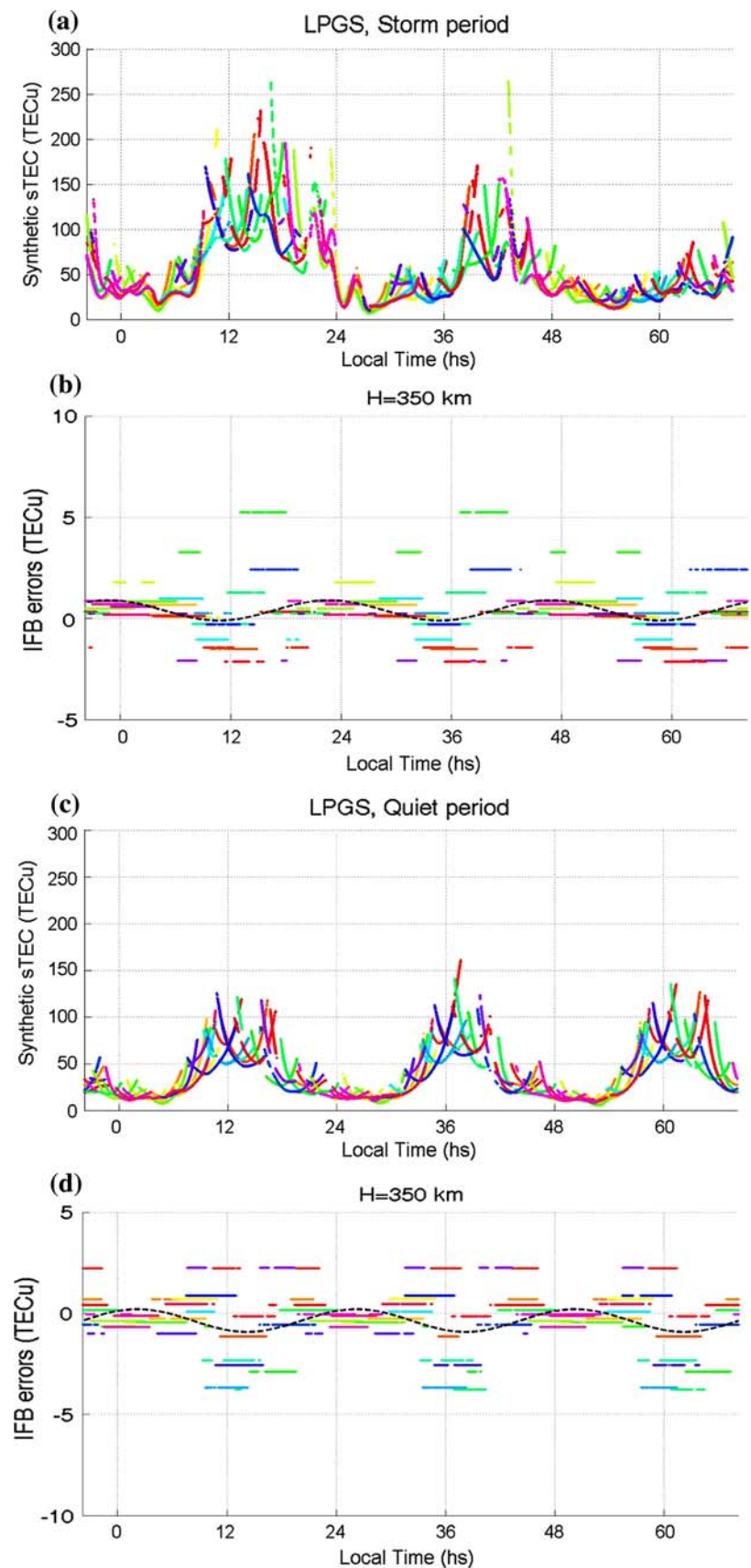
Figure 9 provides a summary of the results obtained for the other stations studied in this work. The left panel of the figure presents the results for the storm period while the right panel presents the results for the quiet period. The comparison between both panels indicates that the IFB errors for the two stations situated to the north of the geomagnetic equator

(the stations are ordered from north to south in the figure) are considerably large; while the IFB errors during the storm and quiet periods are comparable for the remaining three stations. These distinct behaviors are consistent with the fact that continental United States was the region that was most affected by the October 2003 super-geomagnetic storm (Datta-Barua et al. 2005).

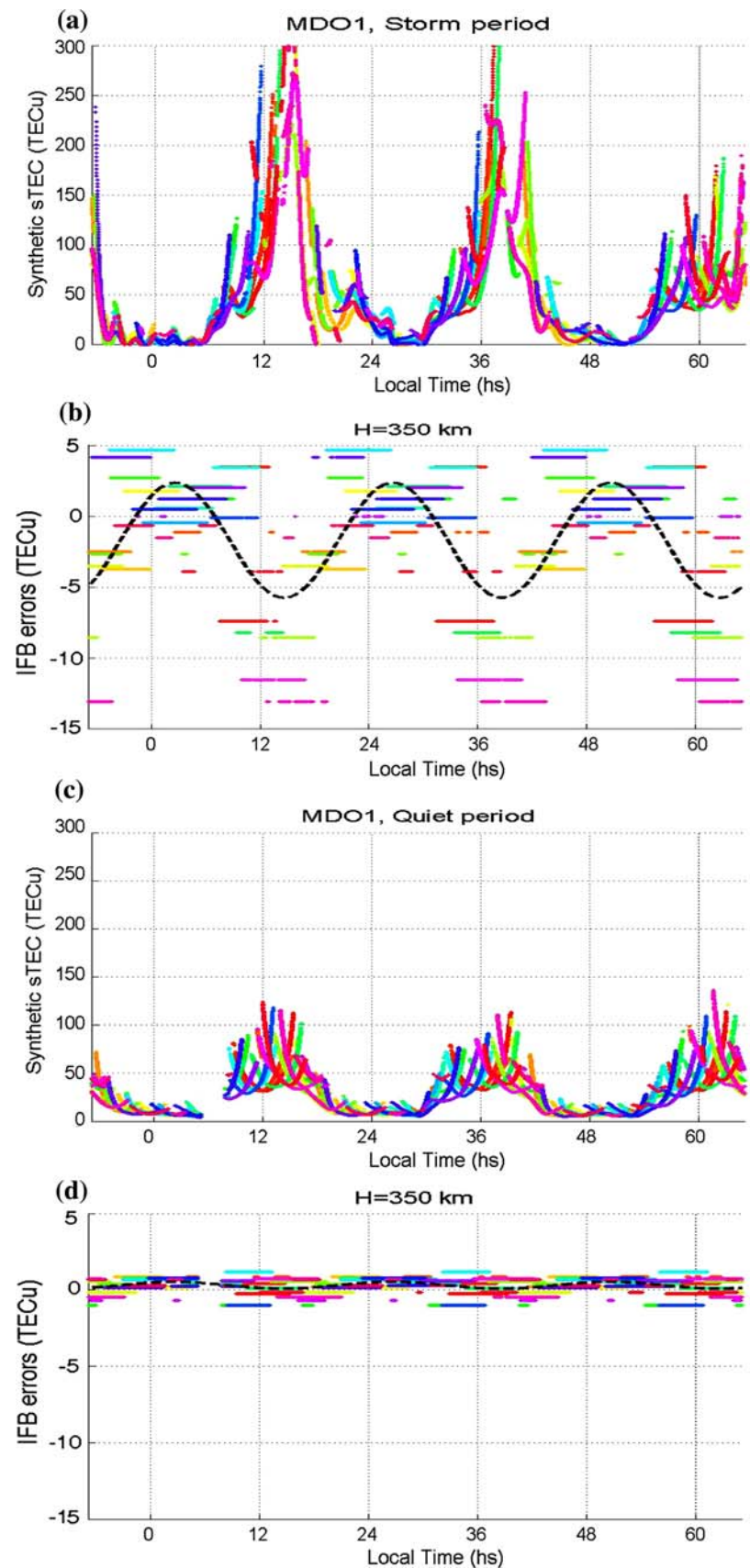
#### 4 Summary and conclusions

The most challenging configuration for the IFB estimation technique corresponds to the station situated in the low geomagnetic region during the period of high solar activity. According to the left panel of Fig. 6c it seems difficult to

**Fig. 7** Synthetic dataset and IFB errors estimated using a thin layer height of 350 km for LPGS, during the storm (*panels a and b*) and the quiet (*panels c and d*) periods; different colors correspond to different satellites



**Fig. 8** Synthetic dataset and IFB errors estimated using a thin layer height of 350 km for MDO1, during the storm (*panels a and b*) and the quiet (*panels c and d*) periods; different colors correspond to different satellites



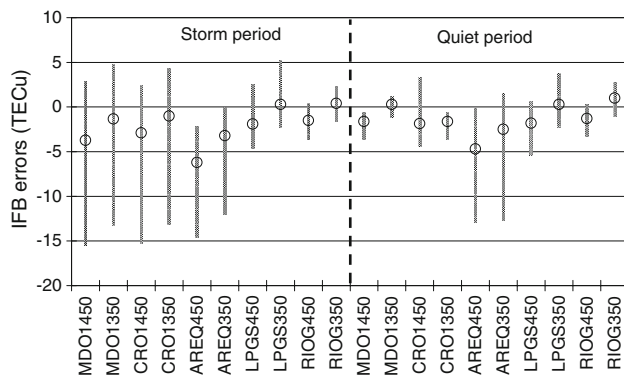


**Fig. 9** Average IFB error (circles) and IFB error interval that contains 95% of the observations (bars) for AREQ, LPGS and RIOG, for storm (left hand side of the figure) and quiet (right hand side of the figure) time; the thin layer height used for the IFB estimation is labeled after the site name

warrant an sTEC accuracy level better than 10 TECu for this particular configuration. This result was expected since the TEC in this situation presents the highest geographical gradients, and thus it significantly reduces the capability of the single-layer approximation and the bi-linear representation to adequately represent the TEC distribution.

The right panels of Fig. 6 indicate that for the low solar activity period, the accuracy level can be considered to be in the order of  $\pm 2$  TECu, even over the low geomagnetic region and with no significant systematic bias affecting the estimations.

As was mentioned in the Introduction to this work, a sensitive parameter involved in the IFB estimation process based on the SLM is the height of the shell. W.r.t. the results shown in Fig. 6 panel c), during the period of high solar activity, a better value for the height for the low geomagnetic region could be closer to 350 km. Figure 6, panels b) and d) suggest that a similar conclusion could be applied for the mid-geomagnetic latitude region, but the effect is not as important as in the low geomagnetic region. For the low solar activity period, the results obtained show no significant evidence in favor of any particular height value.

Finally, the results obtained during a very strong and unusual geomagnetic storm with sTEC values three times larger than expected, like the one that occurred during October 29–31, 2003, show that over the region most affected by the perturbation, the errors on the IFB could be larger than 15 TECu as can be seen in the right panel of Fig. 9. This means that the rates of change of the sTEC for this particular moment and over this region are higher than the one that the IFB technique is able to manage. In contrast, over the region where the storm produces a relative moderate effect, it comes out that although the sTEC values are two times larger than for the quiet period (like over LPGS), the accuracy of the estimated IFB is comparable in both cases.

**Acknowledgments** The authors like to thank the Editors and the reviewers of the manuscript, in particular Dr. Mattia Crespi, for their comments and suggestions that have enhanced the quality and presentation of our work.

## References

- Azpilicueta F, Brunini C (2008) Analysis of the bias between TOPEX and GPS  $\nu$ TEC determinations. *J Geodesy*. doi:10.1007/s00190-008-0244-7
- Azpilicueta F, Brunini C, Radicella S (2005) Global ionospheric maps from GPS observations using modip latitude. *JASR*. doi:10.1016/j.asr.2005.07.069
- Belehaki A, Jakowski N, Reinisch BW (2003) Comparison of ionospheric ionization measurements over Athens using ground ionosonde and GPS derived TEC values. *Radio Sci* 38(6):1105
- Bilitza D, Hernandez-Pajares M, Juan JM, Sanz J (1998) Comparison between IRI and GPS-IGS derived electron content during 1991–1997: first results. *Phys Chem Earth* 24(4):311–319
- Bishop G, Walsh D, Daly P, Mazzella A, Holland E (1994) Analysis of the temporal stability of GPS and GLONASS group delay correction terms seen in various sets of ionospheric delay data. In: *Proceeding ION GPS-94*, pp 1653–1661
- Brunini C, Azpilicueta F (2009) Accuracy assessment of the GPS-based slant total electron content. *J Geod* 83(8):773–785
- Ciraolo L, Azpilicueta F, Brunini C, Meza A, Radicella SM (2007) Calibration errors on experimental slant total electron content determined with GPS. *J Geod* 81(2):111–120. doi:10.1007/s00190-006-0093-1
- Ciraolo L, Spalla C (1997) Comparison of ionospheric total electron content from the Navy Navigation Satellite System and GPS. *Radio Sci* 32(3):1071–1080
- Conker R, El-Arini MB (1998) A novel approach for an ionospheric obliquity process responsive to azimuthal variation. Presented at the ION-GPS-98, Nashville
- Datta-Barua S, Walter T, Konno H, Blanch J, Enge P, Komjathy A (2005) Verification of low latitude ionosphere effects on WAAS during October 2003 geomagnetic storm. In: *Proceedings of the ION 61st annual meeting*, pp 429–439
- Davies K, Hartmann GK (1997) Studying the ionosphere with the Global Positioning System. *Radio Sci* 32(4):1695–1703
- Gao Y (2008) GNSS biases, their effect and calibration. Presented at IGS Analysis Center Workshop 2008, Miami Beach, 2–6 June 2008. <http://www.ngs.noaa.gov/IGSWorkshop2008/prog.html>
- Goposchkin EM, Coster AJ (1992) GPS L1–L2 bias determination. In: *Proceeding international Beacon satellite symposium*, Massachusetts
- Hernández-Pajares M, Juan JM, Sanz J, Orus R, Garcia-Rigo A, Feltens J, Komjathy A, Schaer SC, Krankowski A (2008) The IGS VTEC maps: a reliable source of ionospheric information since 1998. *J Geodes*. doi:10.1007/s00190-008-0266-1
- Ho CM, Wilson BD, Manucci AM, Linqwister UJ, Yuan DN (1997) A comparative study of ionospheric total electron content measurements using global ionospheric maps of GPS, TOPEX radar and the Bent model. *Radio Sci* 32(4):1499–1512
- Jakowski N, Sardon E, Schüter S (1998) GPS-Based TEC observations in comparison with IRI95 and the European TEC model NTCM2. *Adv Space Res* 22(6):803–806
- Jodogne JC, Nebdi H, Warnant R (2004) GPS TEC and ITEC from digisonde data compared with NEQUICK model. *Adv Space Res* 2:269–273
- Manucci AJ, Iijima BA, Lindqwister UJ, Pi X, Sparks L, Wilson BD (1999) GPS and ionosphere: URSI reviews of Radio Science, Jet Propulsion Laboratory, Pasadena

- Mosert M, Gende M, Brunini C, Ezquer R (2007) Comparisons of IRI TEC prediction with GPS and digisonde measurements at Ebro. *Advances in Space Research*, Elsevier, pp 841–847. doi:[10.1016/j.asr.2006.10.02039](https://doi.org/10.1016/j.asr.2006.10.02039)
- Nava B, Coisson P, Miró Amarante G, Azpilicueta F, Radicella SM (2005) A model assisted ionospheric electron density reconstruction method based on vertical TEC data ingestion. *Ann Geophys* 48(2):313–320
- Radicella SM, Leitinger R (2001) The evolution of the DGR approach to model electron density profiles. *JASR* 27(1):35–40
- Rawer K (ed) (1984) *Encyclopedia of Physics, geophysics III: part VII*. Springer, Berlin, pp 389–391
- Sahai Y, Fagundes PR, Becker-Guedes F, Bolzan MJA, Abalde JR, Pillat VG, de Jesus R, Lima WLC, Crowley G, Shiokawa K, MacDougall JW, Lan HT, Igarashi K, Bittencourt C (2005) Effects of the major geomagnetic storms of October 2003 on the equatorial and low-latitude F-region in two longitudinal sectors. *J Geophys Res* 110:A12S91. doi:[10.1029/2004JA010999](https://doi.org/10.1029/2004JA010999)
- Sardon E, Rius A, Zarraoa N (1994) Estimation of the transmitter and receiver differential biases and the ionospheric total electron content from global positioning system observations. *Radio Sci* 29:577–586
- Schaer S (1999) Mapping and predicting the Earth's ionosphere using the Global Positioning System, PhD Thesis of Bern University, 164 p
- Schaer S (2008) Differential Code Biases (DCB) in GNSS Analysis. Presented at IGS Analysis Center Workshop 2008, Miami Beach, 2–6 June 2008. <http://www.ngs.noaa.gov/IGSWorkshop2008/prog.html>